Journal of Environmental Chemical Engineering 14 (2026) 123082

Contents lists available at ScienceDirect

Journal of Environmental Chemical Engineering

journal homepage: www.elsevier.com/locate/jece

pH-dependent self-enhanced decomplexation mechanism of Cu(II)-EDTA in UV/peroxydisulfate system: Reinterpreting the traditional autocatalysis hypothesis

Zhe Xu [a,b,*], Jiantong Zhou [a,b], Chengfeng Liu [a,b], Weilan Zhen [b], Taicheng An [a,b]

[a] Guangdong Key Laboratory of Environmental Catalysis and Health Risk Control, Guangdong-Hong Kong-Macao Joint Laboratory for Contaminants Exposure and Health, Institute of Environmental Health and Pollution Control, Guangdong University of Technology, Guangzhou 510006, China
[b] School of Environmental Science and Engineering, Guangdong University of Technology, Guangzhou 510006, China

ARTICLE INFO

Editor: <Natan Padoin>

Keywords:
Cu(II)-EDTA
UV/peroxydisulfate
Self-enhanced decomplexation
Cu(II) Photoreduction
In-situ hydrolysis and aging

ABSTRACT

The peroxodisulfate (PDS)-based oxidation systems are promising for Cu(II) complex decomplexation owing to its capacity to harness the self-enhanced decomplexation (SED) effect of Cu(II) complexes. This phenomenon was conventionally attributed to liquid-phase autocatalysis via Fenton-like reactions between daughter Cu(II) species and PDS. However, this frequently adopted hypothesis is inconsistent with the actual catalytic activity of Cu(II) species and has been challenged by our preliminary results. Herein, we revisit the decomplexation of copper(II)-ethylenediaminetetraacetate (Cu(II)-EDTA) in UV/PDS system, with particular emphasis on correcting the catalytic behaviors of Cu species and clarifying the indispensable role of UV-irradiation in SED effect. Both acidic and alkaline conditions exhibit significant SED effect, but we reveal a pH-dependent SED mechanism that is fundamentally different from the prevailing liquid-phase autocatalysis mechanism. Under acidic conditions, Cu(II) complexes exhibit enhanced catalytic capacity with decreasing ligand coordination strength, primarily stemming from the activation of PDS by Cu(I) species produced via the irradiation-induced intramolecular charge transfer; In alkaline environments, only liberated Cu(II) substantially contribute to SED effect via spontaneous hydrolysis, forming nanostructured CuO after aging, which activates PDS through heterogeneous Fenton-like processes. While acidic conditions demonstrate faster decomplexation, alkaline-generated solid products facilitate multi-cycle treatment efficiency and alkaline conditions also exhibits stronger resistance to chloride. This work corrects the misinterpretation of SED mechanism in UV/PDS/Cu(II)-EDTA system, and provides a fundamental and accurate mechanistic basis for the efficient treatment of copper-containing organic wastewater by PDS-based processes.

1. Introduction

Heavy metal-organic complexes are widely present in electroplating, leather tanning, printed circuit board manufacturing, and other industrial wastewaters [1-3]. The electroplating sector consumes over one million tons of copper per year, with a substantial fraction released into wastewater as stable metal-organic complexes, making copper recovery from such complex wastewater highly meaningful from both environmental and economic perspectives [4–6]. Copper (II)-ethylenediaminetetraacetate (Cu(II)-EDTA) represents one of the most typical and refractory complexes owing to its high thermodynamic stability, strong chelation affinity, and poor biodegradability. This stable chelated structure prevents direct precipitation or adsorption of Cu^{2+}, rendering conventional water treatment technologies inefficient for decomplexation and metal recovery [7,8]. Consequently, developing effective processes to destroy the chelation structure and release free copper ions has become a key research focus in the treatment of complex-laden wastewaters [9–11].

Oxidative destruction has become the prevailing technique for decomplexation of heavy metal-organic complexes [7,12,13]. In recent years, self-enhanced decomplexation (SED) effect has garnered attention for its ability to remarkably enhance reaction kinetics [14–18]. Our previous work demonstrated that the UV/PDS system is highly efficient for the decomplexation of Cu(II)-EDTA, and a pronounced self-enhanced

* Corresponding author at: Guangdong Key Laboratory of Environmental Catalysis and Health Risk Control, Guangdong-Hong Kong-Macao Joint Laboratory for Contaminants Exposure and Health, Institute of Environmental Health and Pollution Control, Guangdong University of Technology, Guangzhou 510006, China.
E-mail address: zxu@gdut.edu.cn (Z. Xu).

https://doi.org/10.1016/j.jece.2026.123082
Received 17 March 2026; Received in revised form 7 May 2026; Accepted 7 May 2026
Available online 9 May 2026

decomplexation (SED) effect was identified during the reaction based on accelerated kinetics and intensified signals of •OH and $SO_4^{\bullet-}$ in EPR spectra [19]. In that study, EPR characterization showed that the daughter Cu(II) species (such as copper(II)-ethylenediaminediacetate (Cu(II)-ED2A), copper(II)-ethylenediaminemonoacetate (Cu(II)-EDMA), and Cu^{2+}) generated from decomplexation could activate PDS to produce •OH and $SO_4^{\bullet-}$, whereas no obvious radical signals were detected in the pristine Cu(II)-EDTA/PDS system under dark conditions. Accordingly, the homogeneous Fenton-like catalytic reaction of these daughter Cu(II) intermediates with PDS was initially proposed as the cause of the SED effect, and this interpretation has been frequently adopted in later related studies [15,20].

However, this conclusion has been challenged by our subsequent experimental observations, as we found that the major daughter Cu(II) species derived from Cu(II)-EDTA cannot effectively activate PDS to trigger decomplexation or degradation of model organic pollutants [7]. This discrepancy indicates that the traditional interpretation of the SED mechanism is incomplete and lacks rigorous validation. The key limitations include: First, EPR only qualitatively shows that daughter Cu(II) species activate PDS more strongly than Cu(II)-EDTA in the dark. It cannot quantify whether this activity is sufficient to drive efficient decomplexation, so quantitative evaluation is lacking. Second, the formation pathways of •OH and $SO_4^{\bullet-}$ have not been rigorously examined, and the interaction mechanisms between different Cu(II) species and PDS remain unclear. Third, the photochemical behavior of Cu(II) species has not been thoroughly explored. Copper complexes in general are known to possess certain photochemical activity [21–23]. Upon light excitation, such complexes can be promoted to excited states [2,24–27], which in turn alters their chemical behaviors [17,28,29]. Although such photochemical effects are conceptually recognized [17,30–33], they have not been systematically incorporated into the mechanistic framework for Cu(II)-EDTA decomplexation in the UV/PDS system. Such imperfection in the mechanistic understanding limits the rational design and efficient application of PDS-based technologies for complex wastewater treatment.

Furthermore, systematic investigations on Cu(II)-EDTA decomplexation in the UV/PDS system have been performed under acidic conditions [10,19], while overlooking the critical role of alkaline environments that are widely present in real industrial effluents and pre-treated wastewater. Under alkaline conditions, the liberated Cu^{2+} and weakly coordinated Cu(II) species generated from decomplexation can undergo spontaneous hydrolysis and precipitation. This gives rise to heterogeneous reactions such as photocatalysis [14], heterogeneous Fenton-like processes [34], and adsorption. Consequently, the decomplexation characteristics and mechanisms of copper complexes by UV/PDS in alkaline matrices are expected to be fundamentally different from those under acidic conditions. To date, systematic investigations under alkaline conditions remain very limited.

Given the above critical scientific problems and knowledge gaps, this work systematically reinvestigates the decomplexation of Cu(II)-EDTA in the UV/PDS system, aiming to (1) verify the inadequacy of the conventional interpretation on the SED effect; (2) reveal and compare the decomplexation behaviors under acidic and alkaline conditions; (3) explore the in-depth decomplexation mechanisms, including identification of catalytically active Cu species, characterization of reactive oxygen species, elucidation of decomplexation pathways, and uncovering the molecular-level mechanism of the SED effect. Overall, this work provides an accurate and reliable mechanistic basis for the practical application of UV/PDS processes in the treatment of copper-complex-containing industrial wastewater.

2. Experimental

2.1. Chemicals and reagents

All reagents were of analytical grade or higher purity and were used without further purification upon receipt. $CuSO_4•5H_2O$, PDS and EDTA were purchased from Sigma-Aldrich. Cu(II)-EDMA was bought from Tokyo Chemical Industry. 5,5-dimethyl-1-pyrroline N-oxide (DMPO) and 2,2,6,6-tetramethylpiperidine (TEMP) were obtained from J&K Chemical. Rhodamine B (RhB), chloroform ($CHCl_3$), methanol, tert-butanol (TBA), furfuryl alcohol (FFA), sodium hydroxide (NaOH), sodium sulfite (Na_2SO_3), sodium chloride (NaCl), sodium nitrate ($NaNO_3$), sodium periodate ($NaIO_4$), neocuproine, iminodiacetic acid (IDA), nitrilotriacetic acid (NTA) and other reagents were provided by Aladdin.

2.2. Decomplexation efficiency assessment

The experimental procedure was conducted as follows: A predetermined concentration of Cu(II)-EDTA solution was introduced into a quartz reactor, followed by the addition of PDS. The pH was then adjusted to the target value using HNO_3 and NaOH. The reactor was subsequently positioned 12 cm from the light source (measured from the center of the cylindrical reactor to the outer surface of the UV lamp). A low-pressure mercury lamp (10 W, 254 nm, Heraeus) was employed as the UV source, with a preheating period exceeding 15 min prior to reaction initiation. The radiometer shows an irradiance of 1.8 mW•cm^{-2}. Throughout the reaction, the solution pH was maintained at the set value by HNO_3 and NaOH. At predetermined time intervals, samples were withdrawn and immediately quenched with 0.2 mol•L^{-1} sodium sulfite to prevent further ligand oxidation. pH of each sample was then raised to 11.0 to precipitate free Cu^{2+} and weakly bound Cu(II) species. After 3 h of precipitation, the residual Cu concentration (representing the remaining complexed copper) in the supernatant was quantified via atomic absorption spectroscopy (Shimadzu, AA7700). All dark reactions and light/dark cycling experiments were performed under identical conditions, with the exception of light modulation using a shading plate. In a typical process, the initial concentration of Cu(II)-EDTA was set to be 0.6 mmol•L^{-1} based on the actual water quality of the metal processing wastewater (strongly complexed copper usually ranges from several mg•L^{-1} to nearly 100 mg•L^{-1}). And an initial PDS concentration of 50 mmol•L^{-1} was selected to ensure that there is sufficient PDS to completely decomplex Cu(II)-EDTA.

2.3. Reactive oxygen species analysis

Oxidative species formed during decomplexation was detected via EPR spectroscopy and quenching experiments. For EPR characterizations (Bruker EMXplus), the reaction solution containing 0.6 mmol•L^{-1} Cu(II)-EDTA, 50 mmol•L^{-1} PDS and capturer was encapsulated in capillaries and placed on the sample stage under irradiation from a medium-pressure mercury lamp. EPR spectra were acquired at early and middle stages (1.5 and 5 min for acidic conditions; 5 and 10 min for alkaline conditions). Hydroxyl radicals (•OH), sulfate radicals ($SO_4^{\bullet-}$), and superoxide anions ($O_2^{\bullet-}$) were trapped by DMPO, while singlet oxygen ($^1O_2$) was probed using TEMP. Quenching experiments followed a protocol similar to that of the decomplexation assay, except that scavengers were added prior to illumination. These included TBA (•OH-specific quencher), methanol (reacting with •OH, $SO_4^{\bullet-}$), and FFA (non-selective quenchers for both homogenous and heterogeneous oxidation).

2.4. Cu speciation and oxidation state analysis

The concentrations of Cu(II)-EDTA and daughter complexes, including copper(II)-ethylenediamine triacetate (Cu(II)-ED3A), Cu(II)-ED2A and Cu(II)-EDMA, were quantitatively determined by HPLC. The detection conditions were consistent with previous studies [7,35]. Cu(III) was probed via periodate method [36,37]. Cu(I) was measured using the neocuproine (NCP) assay under identical conditions (detection wavelength of 458 nm). The experimental procedures for monitoring Cu(I) and Cu(III) concentrations during the reaction are as follows. To prevent rapid quenching of unstable Cu(I) and Cu(III) after ceasing

illumination, NCP or sodium periodate was added to the solution under continuous UV irradiation. After mixing for 10 s, the sample was transferred to darkness, and the absorbance was measured after 5 min. For analyzing the formation of Cu(I) and Cu(III) by individual Cu(II) species, the concentration of each Cu(II) species was increased to 2.4 mmol•L^{-1} to minimize the fraction of oxidized species, thereby suppressing interference from further transformation into other Cu(II) species. After adding NCP or sodium periodate, the UV light was turned on to initiate the reaction. The chromogenic reagent continuously captured the generated Cu(I) and Cu(III). After 60 s of reaction, the light was stopped, and UV–vis absorption spectra were recorded to reflect the accumulated amounts of Cu(I) and Cu(III). The calibration curves for Cu (I) and Cu(III) are provided in Fig. S1.

2.5. Cu species catalytic activity assessment

The catalytic activity of aqueous Cu(II) species was evaluated by monitoring the degradation of RhB in Cu(II) species/PDS systems. The concentration of RhB was measured by HPLC according to the reported method [38]. The initial concentrations of Cu(II) species, PDS and RhB were 0.001 mmol•L^{-1}, 0.1 mmol•L^{-1} and 0.01 mmol•L^{-1}, respectively. To quantitatively analyze the catalytic activity of each species, the degradation rates of RhB in the PDS alone and Cu(II) species/PDS systems were measured under both illumination and dark conditions, allowing the contributions of direct PDS oxidation, UV/PDS, and photo-assisted Fenton-like catalysis by Cu(II) species to be calculated and distinguished. To demonstrate the catalytic properties of solids produced during the decomplexation under alkaline conditions, we tested RhB degradation by heterogeneous photocatalysis and Fenton-like. In each experiment, the concentrations of the solid, PDS and RhB were 50 mg•L^{-1}, 0.1 mmol•L^{-1} and 0.01 mmol•L^{-1}, respectively.

2.6. DFT calculations

DFT enables us to obtain molecular-level insights into the behavior of key species that are difficult to capture experimentally, thereby providing theoretical support for understanding the underlying mechanism.

All parameters related to the DFT calculations in this study were selected in accordance with the calculation specifications for transition metal-organic complex systems, the experimental reaction environment, and the principle of balancing accuracy and efficiency. Specifically, the calculations were performed using the Gaussian 09 software. The B3LYP-D3 (BJ) functional was adopted: the B3LYP hybrid functional can accurately describe the coordination bonds, valence state cycles (Cu (I)/Cu (II)/Cu (III)), and free radical reactions of copper complexes, while the D3 (BJ) dispersion correction can effectively make up for the deficiency of traditional functionals in describing intramolecular non-covalent interactions and van der Waals forces. A mixed basis set strategy was employed: the Lanl2TZ (f) pseudopotential basis set was used for copper atoms, which not only takes into account the correction of relativistic effects and the description of 3d orbital polarization but also greatly reduces the calculation cost of heavy atoms, adapting to the core needs of copper valence evolution and coordination activation. The def2-TZVPP all-electron basis set was used for light atoms such as C, H, O, N, and S, which can accurately describe the electronic structures of organic ligands, active free radicals. Meanwhile, an implicit water solvent model was adopted to match the experimental aqueous reaction environment.

3. Results and discussion

Decomplexation kinetics and SED phenomenon

We initially evaluated the decomplexation of Cu(II)-EDTA by UV/PDS process at pH 3.0 and 10.0 (Fig. 1a). The results demonstrated superior performance at both pHs, with acidic condition exhibiting higher kinetics (90% decomplexation achieved in ~15 min) compared to alkaline environment (~28 min). Notably, both conditions exhibited pronounced SED phenomena, as evidenced by the removal profiles of copper, EDTA, and total organic carbon (TOC) (Fig. S2 and S3), showing an initial slow removal period (induction stage) followed by a fast decomplexation stage. According to TOC reduction, the induction stages lasted for 3 min and 9 min under acidic and alkaline conditions, respectively. Prior investigations have hypothesized that the SED effect in PDS-based systems associated with a mechanistic transition in decomplexation, from initial energy-driven activation to dual energy and daughter complexes/Cu^{2+} co-activation, with the decomplexation intermediate/product activation becoming dominant after several min of reaction [19]. Light-on/off experiments were conducted to verify this hypothesis. Contrary to expectations, interrupting illumination after the induction period resulted in significant decomplexation suppression in both conditions (Fig. 1b), particularly in acidic environments where decomplexation almost ceased in darkness. These findings suggest that the traditional autocatalysis hypothesis cannot explain the observed SED.

To elucidate the mechanistic basis of SED effect, we analyzed the daughter Cu(II) complexes during the decomplexation (Fig. S4). Both acidic and alkaline conditions predominantly generated decarboxylation products including Cu(II)-ED3A, Cu(II)-ED2A, and Cu(II)-EDMA, with trace Cu(II)-NTA detected (and Cu(II)-IDA in acidic conditions).

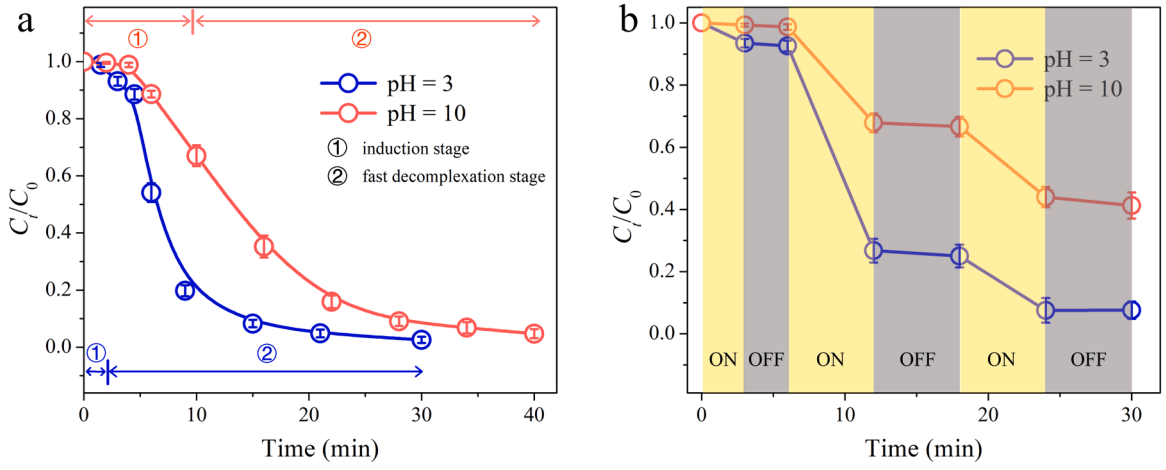

Fig. 1. Decomplexation efficiency of Cu(II)-EDTA in UV/PDS process under (a) continuous irradiation and (b) light-dark cycle conditions ($[Cu(II)\text{-}EDTA]_0$ = 0.6 mmol•L^{-1}, $[PDS]_0$ = 50 mmol•L^{-1}).

However, obvious differences in product distribution were observed. Under acidic conditions, Cu(II)-EDTA, Cu(II)-ED3A and Cu(II)-ED2A were rapidly decomposed, while Cu(II)-EDMA accumulated. At 5 min (46% decomplexation), signals for Cu(II)-EDTA, Cu(II)-NTA, and Cu(II)-ED3A nearly vanished, leaving strong Cu(II)-EDMA and weak Cu(II)-IDA and Cu(II)-ED2A signals. In contrast, alkaline conditions maintained more balanced degradation of intermediates, with detectable Cu(II)-EDTA and Cu(II)-ED3A even at 68% decomplexation. These divergent product distributions reflect different ligand degradation selectivity, implying fundamentally distinct decomplexation mechanisms between acidic and alkaline environments.

3.1. Identification of reactive oxygen species

The decomplexation mechanism was further probed by EPR and quenching experiments to characterize the oxidative species. EPR spectra revealed signals of •OH, $SO_4^{\bullet-}$, and $^1O_2$ in the induction stage, with comparable intensities observed at both pHs (Fig. 2a and b). Notably, upon progression to the fast decomplexation stage, a pronounced enhancement in ROS concentrations was observed under acidic conditions, with •OH exhibiting the most significant amplification, suggesting an intensified generation pathway for •OH during the decomplexation. As the reaction proceeds, the signal intensity of •OH began to decline. On the contrary, ROS signals did not intensify under alkaline conditions, reflecting the pH-dependent decomplexation properties. Quenching experiments unequivocally demonstrated the critical role of •OH in decomplexation (Fig. 3), as TBA exerted significant inhibition at both pHs. While methanol further suppressed the decomplexation, implicating the contributory role of $SO_4^{\bullet-}$ in the process. The addition of $CHCl_3$ did not impose significant influence on the decomplexation, reflecting the limited contribution of $O_2^{\bullet-}$. The decomplexation was almost inhibited in the presence of FFA. These findings collectively underscore the involvement of radical and non-radical oxidation pathways. The stronger inhibitory effect of TBA and methanol under acidic conditions hints an alternative oxidative pathway under alkaline conditions.

3.2. Evolution of Cu valence states

To elucidate the role of copper in decomplexation, we assessed the temporal evolution of Cu oxidation state during the reaction. As illustrated in Fig. 4, the Cu(I) concentration increases rapidly in the early stage and reaches a maximum of approximately 0.047 mmol•L^{-1} at 5 min. According to the TOC results (Fig. S2), the solution still contains a high content of small organic acids at this time, and Cu(II) mainly binds with EDMA and its further degraded small-molecule acids. As the reaction proceeds, the Cu(I) concentration undergoes a gradual decay. In contrast, Cu(III) concentration increases monotonically in the first 20 min and then keeps stable. The origin of Cu(I) and Cu(III) species was investigated by testifying their yields by each individual Cu(II) complex. Cu(II)-EDTA, Cu(II)-ED2A, and Cu(II)-EDMA demonstrated comparable Cu(I) yields (Fig. S5a), whereas Cu^{2+} produced negligible Cu(I). This disparity primarily stems from the reductive properties of organic ligands, particularly carboxylate groups [39,40]. The absence of detectable Cu(I) in dark conditions suggests that irradiation-induced intramolecular electron transfer (IET) is the dominant pathway for Cu(I) formation (Fig. S5b). Moreover, the organic radicals generated from ligand oxidation retain reductive capacity, thereby facilitating Cu(II)

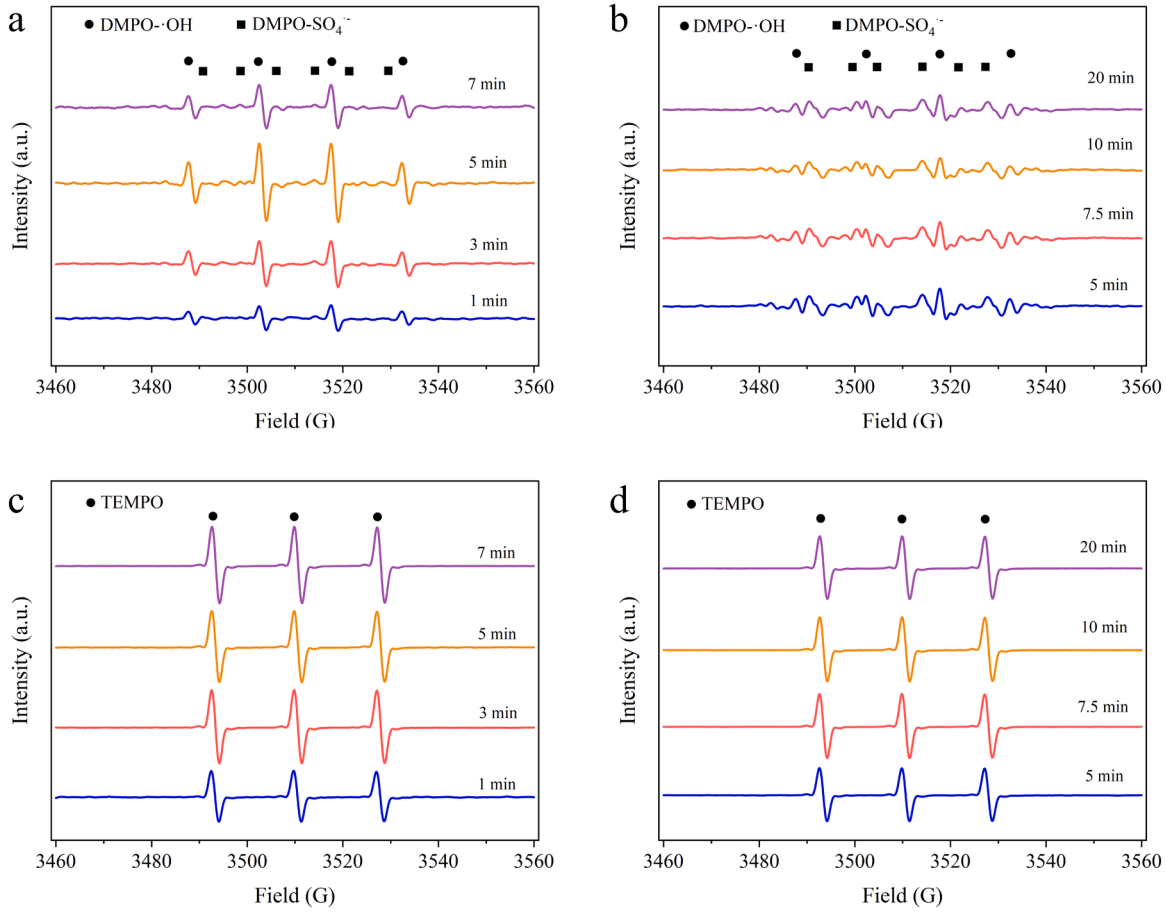

Fig. 2. EPR spectra of the solution at different reaction times. (a, b) Captured using DMPO at pH 3.0 and pH 10.0, respectively; (c, d) Captured using TEMP at pH 3.0 and pH 10.0, respectively ($[Cu(II)\text{-}EDTA]_0 = 0.6$ mmol•L^{-1}, $[PDS]_0 = 50$ mmol•L^{-1}).

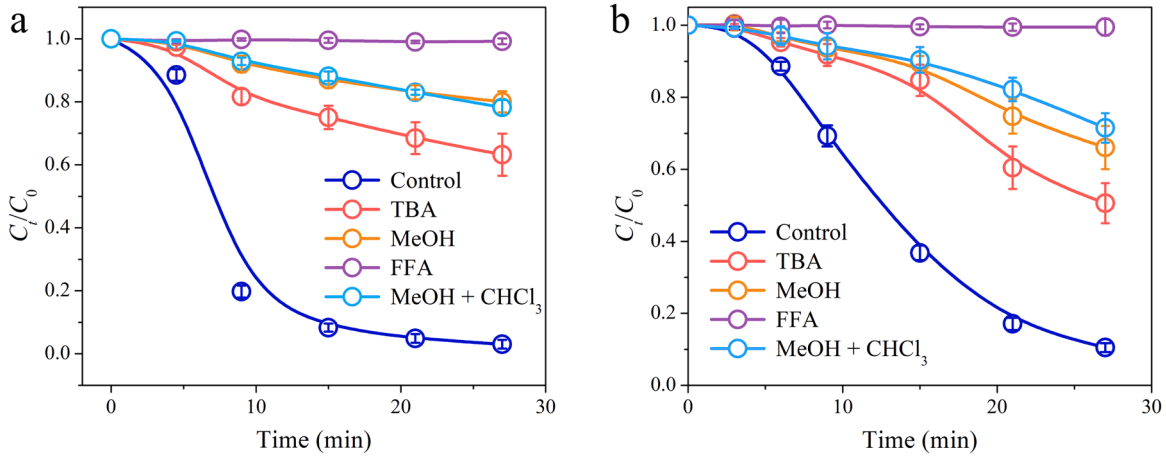

Fig. 3. Quenching experiments at (a) pH 3.0 and (b) pH 10.0, respectively ([Cu(II)-EDTA]$_0$ = 0.6 mmol•L^{-1}, [PDS]$_0$ = 50 mmol•L^{-1}, [quenchers]$_0$ = 0.1 mol•L^{-1}).

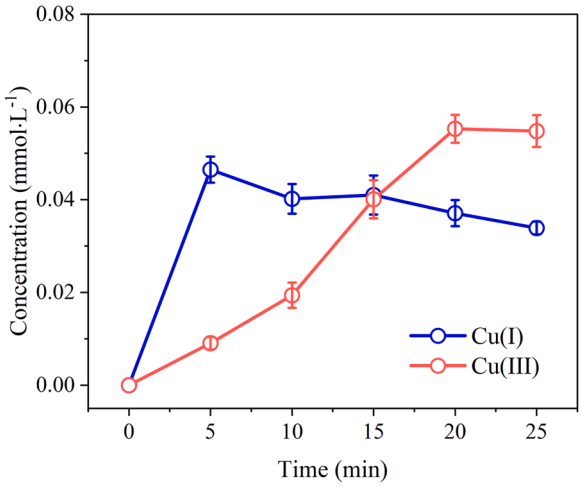

Fig. 4. UV–vis spectra detecting the generation of (a) Cu(I) and (b) Cu(III) during Cu(II)-EDTA decomplexation at pH 3.0 ([Cu(II)-EDTA]$_0$ = 0.6 mmol•L^{-1}, [PDS]$_0$ = 50 mmol•L^{-1}).

reduction [41,42]. Unexpectedly, Cu(III) was exclusively produced by Cu^{2+} rather than Cu(II)-EDTA and daughter Cu(II) complexes (Fig. S6), implying that Cu(III) generation occurs via Cu^{2+}/PDS reactions (Eq. (3)) but not oxygen transfer from Cu(I) precursors. These findings collectively support the SED mechanism described by Eqs. (1–4) where PDS was activated through Cu(II)/Cu(I) cycling. To directly confirm the role of Cu(I) in PDS activation, we tested the degradation of RhB by Cu(I)/PDS and control processes. Hydroxylamine hydrochloride (NH_2OH•HCl), a widely used Cu(II) reducing agent, was employed to generate Cu(I), and the produced Cu(I) was stabilized by NCP. The results show that neither the addition of Cu^{2+} + NCP nor the addition of NH_2OH•HCl + NCP could effectively activate PDS (Fig. S7). Instead, only the combined addition of the three components achieved RhB degradation. This directly proves that Cu(I) species can efficiently activate PDS.

$$Cu(II) - L \xrightarrow{UV} Cu(I) - L\bullet \quad (1)$$

$$PDS \xrightarrow{Cu(I)-L\bullet} SO_4^{\bullet-} + SO_4^{2-} \quad (2)$$

$$Cu^{2+} + PDS \xrightarrow{UV} Cu^{3+} + SO_4^{\bullet-} + SO_4^{2-},\ \Delta G = -53.81\ kJ \bullet mol^{-1} \quad (3)$$

$$SO_4^{\bullet-} + H_2O \rightarrow \bullet OH + SO_4^{2-} + H^+,\ \Delta G = -46.69\ kJ \bullet mol^{-1} \quad (4)$$

To further clarify the role of Cu(II) species in SED, we evaluated RhB degradation efficiencies by different processes. In dark conditions, all systems exhibited limited RhB degradation (Fig. S8), with only Cu^{2+} showing a distinguishable promoting effect. This observation is consistent with the retarded decomplexation without UV irradiation. Under illumination, the main RhB degradation pathways include UV-activated PDS and UV-assisted Fenton-like activation by Cu(II) species. Therefore, the contribution of each pathway can be distinguished based on Fig. 5. The results show that the contribution of the UV-assisted Cu(II)-EDTA activation pathway is already higher than that of UV/PDS, reaching approximately 1.67 times that of UV/PDS. As EDTA degrades into ED2A and EDMA, the activation rate of UV-assisted Cu(II) complexes is greatly enhanced, reaching about 3.59 and 5.92 times that of UV/PDS, respectively (Fig. 5b). Therefore, the decomposition of Cu(II)-EDTA into daughter complexes under acidic conditions promotes PDS activation. However, when the ligand is completely mineralized to Cu^{2+}, its catalytic activity is even lower than that of the UV/PDS pathway, which may reduce the catalytic efficiency in the late reaction stage.

To clarify the intrinsic relationship between the photocatalytic activity of daughter Cu(II) complexes under UV irradiation and the significantly enhanced radical signals in EPR spectra, we investigated the RhB degradation performance in the UV/Cu(II)-EDMA/PDS and UV/Cu(II)-ED2A/PDS systems with methanol as a radical scavenger. As shown in Fig. S9, the addition of methanol drastically suppressed RhB degradation, confirming that radical generation from the photo-assisted activation of PDS by daughter Cu(II) complexes is the main contributor to the SED effect under acidic conditions.

For a deeper insight into the catalytic mechanism of copper complexes, we employed Cu(II)-EDMA as a representative daughter complex, optimizing the molecular structure of its IET-derived Cu(I) complex and calculating the reaction energy with PDS (Fig. 6). Results revealed that EDMA-coordinated Cu(I) can activate PDS to generate $SO_4^{\bullet-}$ ($\Delta G = -376.34$ kJ•mol^{-1}), exhibiting superior thermodynamic feasibility compared to Cu^{2+} activation (Eq. (3), ΔG = -53.81 kJ•mol^{-1}). Notably, $SO_4^{\bullet-}$ preferentially reacts with water to form •OH (Eq. (4)), accounting for the pronounced hydroxyl radical signal observed. Our calculation suggests the binding between PDS and Cu(II)-EDMA (Fig. 4), forming a ternary EDMA-Cu(II)-PDS complex ($\Delta G = -155.71$ kJ•mol^{-1}). In EDMA-Cu(II)-PDS complex, PDS can act as a reductant under light irradiation, facilitating Cu(II)→Cu(I) conversion ($\Delta G = -378.19$ kJ•mol^{-1}) and thus accelerating the Cu(I)/Cu(II) catalytic cycle.

Furthermore, attempts were made to obtain experimental evidences supporting the formation of ternary EDMA-Cu(II)-PDS complex. Using

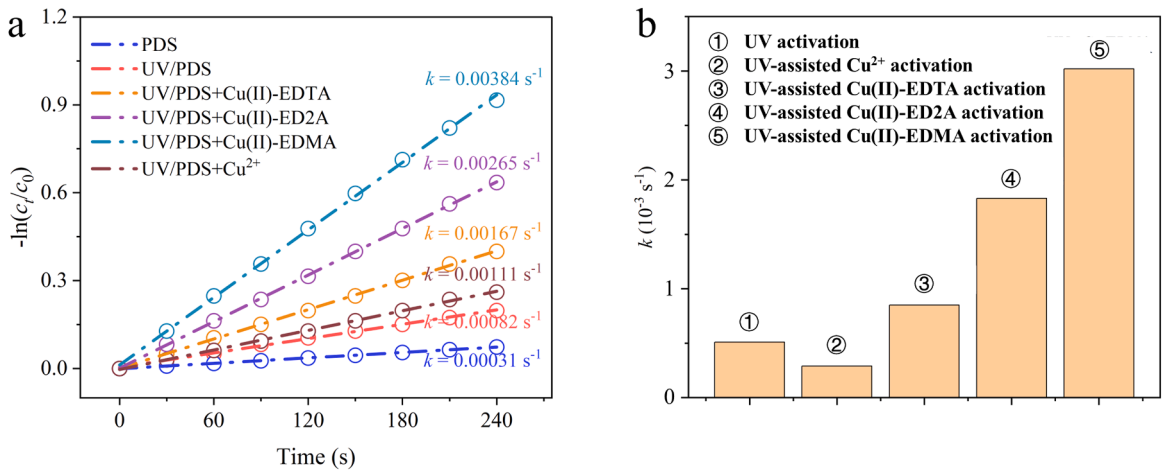

Fig. 5. (a) Degradation kinetics of RhB in different systems and (b) calculated pseudo-first-order rate constants of each pathway ([Cu(II) species] = 0.6 mmol•L^{-1}, [RhB]$_0$ = 6.0 mmol•L^{-1}, [PDS]$_0$ = 50 mmol•L^{-1}, pH = 3.0).

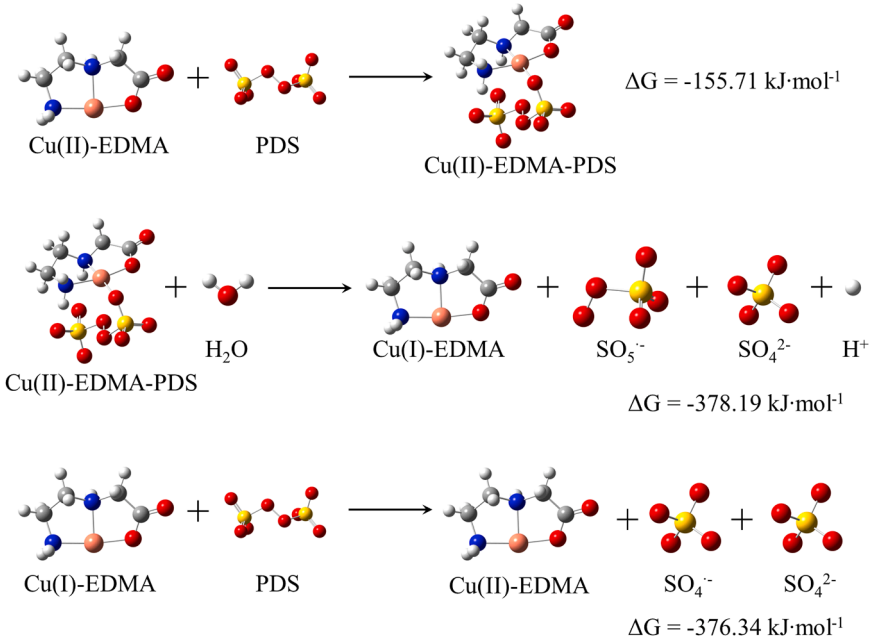

Fig. 6. Calculated molecular structure and free energy reflecting the reactions between Cu(II)-EDMA and PDS (Blue: N, grey: C, while: H, red: O, orange: Cu, yellow: S).

Cu(II)-EDMA as a model species, we compared Cu(I) accumulation kinetics in two systems, UV/Cu(II)-EDMA (System a) and UV/Cu(II)-EDMA/PDS (System b). If Cu(II) existed only as the Cu(II)-EDMA binary complex, the Cu(I) yield in System a and System b would be similar under illumination. Moreover, since PDS can oxidize Cu(I), the Cu(I) concentration in System a should be higher than that in System b. However, our experimental results clearly show that the Cu(I) accumulation rate in System b was faster than in System a (Fig. S10). This observation indicates that PDS actively participates in Cu(I) generation, and its promoting effect on Cu(I) formation outweighs its oxidative consumption of Cu(I). The chelating strength of EDMA toward Cu(II) is much stronger than that of PDS (as EDMA effectively inhibits Cu(II) precipitation under alkaline conditions). Thermodynamically, PDS cannot displace EDMA to form a Cu(II)-PDS binary complex via ligand exchange. Therefore, we propose that the promotion of Cu(I) generation by PDS most likely occurs through the formation of an EDMA-Cu(II)-PDS ternary complex, which facilitates the photoreduction of Cu(II) to Cu(I) under illumination. This pathway is responsible for the accelerated Cu(I) accumulation observed in our experiments.

Under alkaline conditions, the Cu(I) concentration first increases rapidly and reaches a maximum of 0.035 mmol•L^{-1} at 10 min (Fig. 7), which is lower than that under acidic conditions (Fig. 4). Then the Cu(I) concentration decreases slowly. Different from acidic conditions, Cu(II) under alkaline conditions does not form stable complexes with weakly chelating small-molecule acids (which can generate Cu(I) via photochemical processes), but hydrolyzes into solid precipitates. The resulting solids can react with reductive substances (such as $O_2^{\bullet-}$ and organic radicals) or undergo photoreduction to produce Cu(I), which compensates for the loss of Cu(I) caused by the disappearance of Cu(II) complexes. For Cu(III), its accumulation is slow at first but increases sharply after 10 min and then maintains relatively stable after 20 min. The maximum Cu(III) concentration at pH 10.0 (0.108 mmol•L^{-1}) is nearly twice that at pH 3.0 (0.055 mmol•L^{-1}).

Analysis of individual Cu(II) species revealed that Cu(I) generation followed the order of Cu(II)-EDTA > daughter Cu(II) complexes > Cu^{2+} (Fig. S11a). The ambiguous Cu(I) signal in the absence of light indicated

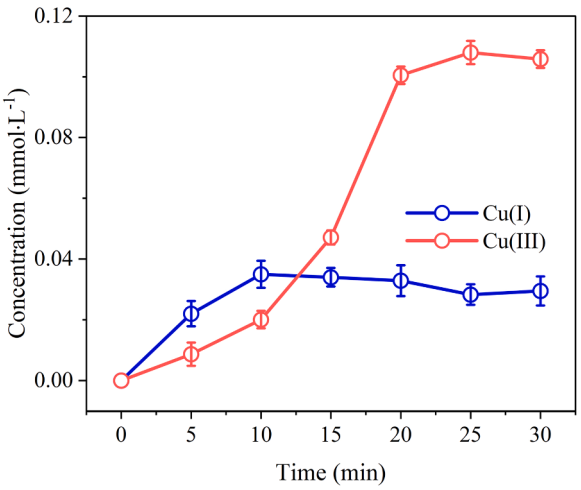

Fig. 7. UV–vis spectra detecting the generation of (a) Cu(I) and (b) Cu(III) during Cu(II)-EDTA decomplexation at pH 10.0 ($[Cu(II)\text{-}EDTA]_0$ = 0.6 mmol•L^{-1}, $[PDS]_0$ = 50 mmol•L^{-1}).

that Cu(I) formation under alkaline conditions also relies on photochemical processes (Fig. S11b), aligning with the negligible Cu(I) signal observed in ligand-free solutions. In comparison to acidic conditions, the decontamination by Cu(I)/PDS system was slower under alkaline conditions, likely due to deprotonation-enhanced Cu(I)-ligand interactions, which stabilized Cu(I) and hindered its reaction with PDS. For Cu(III), however, Cu(II)-EDTA and the daughter Cu(II) complexes exhibited limited Cu(III) signal (Fig. S12). Significant Cu(III) signal only emerged in the absence of ligands, which seems inconsistent with the Cu(III) concentration trajectory where the Cu(III) signal attenuated after 20 min. This discrepancy may arise from the dynamic evolution of Cu(II) species during the spontaneous precipitation of labile Cu(II) under alkaline conditions.

We also quantitatively analyzed the oxidation efficiency of each pathway under alkaline conditions, as shown in Fig. 8. Compared with acidic conditions, the degradation rates of most pathways under alkaline conditions are slowed down. The degradation rate of the UV/PDS pathway is only about 55% of that under acidic conditions. In particular, the efficiency of UV-assisted Cu(II) complex-activated PDS is significantly reduced and lower than the UV/PDS pathway. The freshly formed Cu(II) precipitate also shows negligible catalytic activity (only 6% of the UV/PDS pathway). Only the aged Cu(II) precipitate exhibits outstanding PDS activation activity, which is 2.87 times that of the UV/PDS pathway. This indicates that the enhanced oxidation activity under alkaline conditions occurs only after the formation of aged Cu(II) precipitates.

3.3. *In-situ hydrolysis, precipitation, and aging of Cu species*

XRD and SEM results indicated that the precipitates with short aging time consisted of light blue amorphous Cu(II) (hydr)oxide nanoparticles, while the precipitates collected at 30 min were featured by brown CuO nanosheets (Figs. 9 and 10). As depicted in Fig. S12, a significant Cu(III) signal was detected in aged precipitates, whereas no such signal was observed for nascent precipitates, suggesting the aging-dependent catalytic properties of the precipitates. We compared RhB degradation in nascent precipitate/PDS and aged precipitate/PDS systems. Results showed that the nascent precipitate exhibited negligible Fenton-like activity (Fig. S13). In contrast, the aged precipitate effectively activated PDS for RhB degradation. This explains the initial enhancement of Cu(III) signals. The subsequent decline in Cu(III) signals can be attributed to further aging of the precipitate, a spontaneous process that reduces system energy and results in the loss of highly active sites and surface area. The solids collected at the end of the decomplexation (pH 10) were then used to treat Cu(II)-EDTA wastewater in the next batch, reducing the time required for 90% decomplexation from 28 to 22 min (Fig. S14), confirming the catalytic role of the precipitate.

To quantitatively evaluate the contribution of solid-phase species under alkaline conditions, the decomplexation reaction was allowed to proceed for 15 min (rapid decomplexation stage), afterward the solution was divided into two portions. One portion continued the

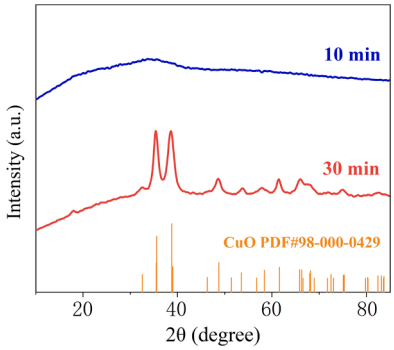

Fig. 9. XRD patterns of the precipitates collected at 10 min and 30 min of reaction.

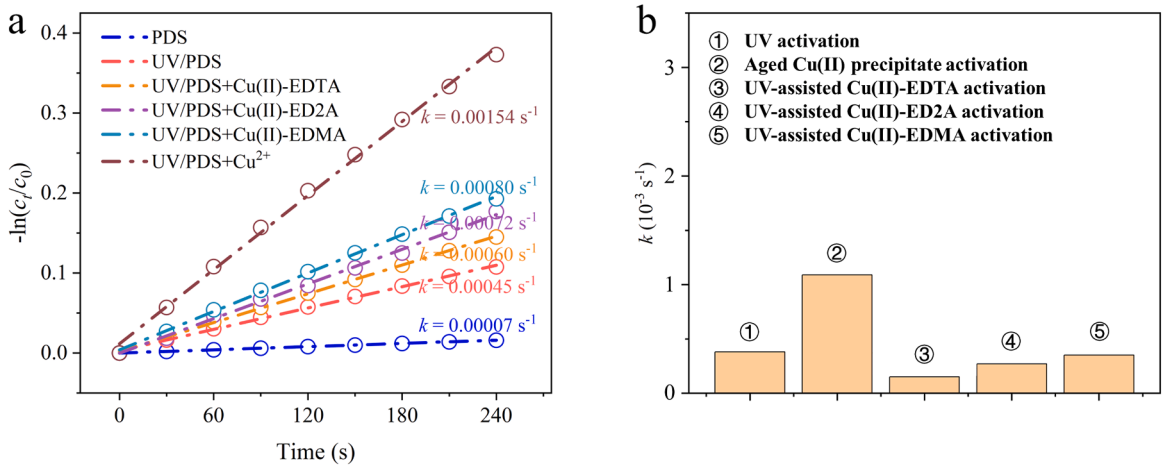

Fig. 8. (a) Degradation kinetics of RhB in different systems and (b) calculated pseudo-first-order rate constants of each pathway ([Cu(II) species] = 0.6 mmol•L^{-1}, $[RhB]_0$ = 6.0 mmol•L^{-1}, $[PDS]_0$ = 50 mmol•L^{-1}, pH = 10.0).

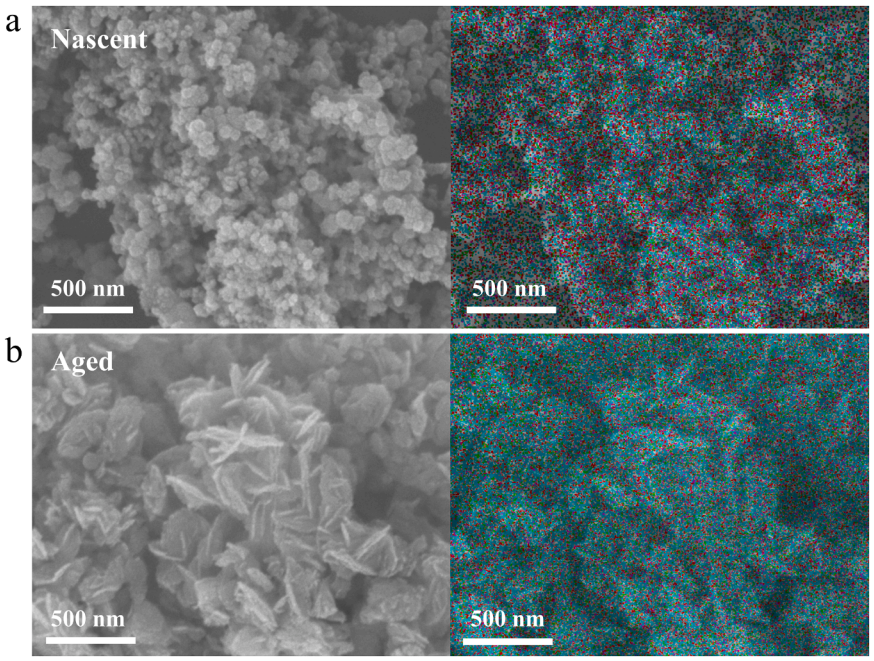

Fig. 10. SEM images of precipitates collected at 10 min and 30 min of reaction (Cu: blue, O: red).

decomplexation process, while the other portion was immediately subjected to vacuum filtration to remove solid species from the solution, followed by UV irradiation of the filtrate. The results show that the decomplexation rate decreased by approximately 56% after the removal of solids (Fig. S15), demonstrating that the in-situ generated solid phase plays a crucial role in the decomplexation process.

Additionally, since CuO is a typical semiconductor material, the photocatalytic performance of the precipitate was investigated (Fig. S16). We found that the photocatalytic degradation rate of RhB was slow, with an apparent rate constant of 0.0016 min^{-1} , significantly lower than that of the Fenton-like catalytic reaction (0.0089 min^{-1}). Furthermore, the decontamination efficiency of the precipitate/UV/PDS system was close to the sum of each individual process (Fenton-like, photocatalysis, and photo-activated PDS), indicating no significant synergistic effect between UV irradiation and Fenton-like process under alkaline conditions. In summary, the SED effect under alkaline conditions is primarily attributed to the Fenton-like catalytic activity of the precipitated solids.

The CuO/PDS Fenton-like system has been investigated in a few studies. Recently, several reports have demonstrated that non-radical pathways (e.g., Cu(III) and Cu(III)-mediated surface electron transfer) serve as important oxidation mechanisms in this system [43,44], which is consistent with the high concentration of Cu(III) observed under alkaline conditions in this work. To verify this quantitatively, methanol

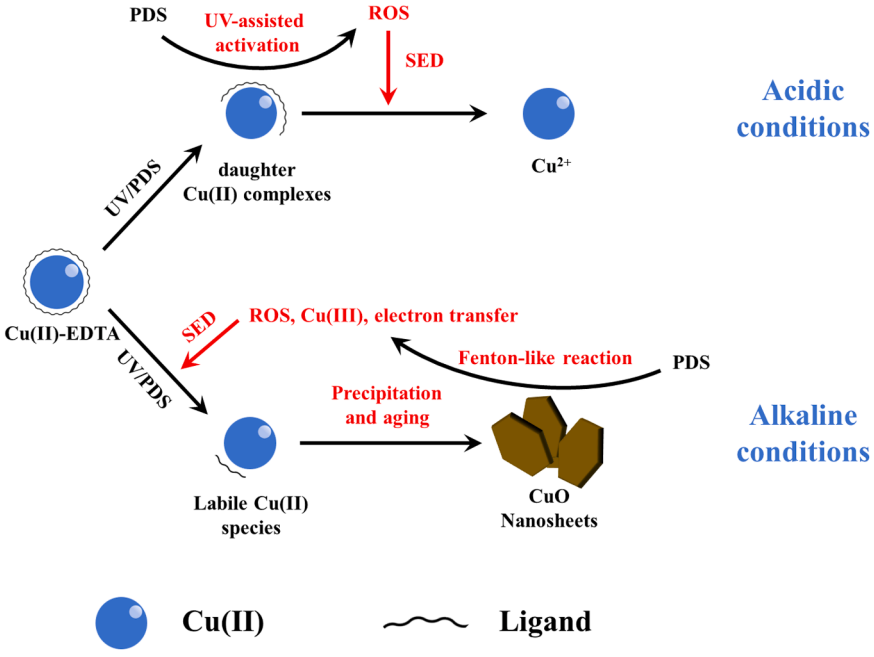

Fig. 11. Schematic diagram of the SED mechanisms under acidic and alkaline conditions (the red-highlighted part represents the new findings of this work that differ from the previous hypothesis).

was added during the rapid decomplexation stage to block the radical pathways. Results showed that decomplexation almost ceased under acidic conditions, whereas it still proceeded under alkaline conditions (Fig. S17), confirming the presence of non-radical decomplexation pathways at alkaline pH. Moreover, the influence of organic pollutants on PDS decomposition was examined to verify the occurrence of surface charge transfer. Compared with the system without organic substrates, the PDS consumption rate was greatly accelerated in the presence of RhB or Cu(II)-EDMA (Fig. S18), which is a typical characteristic of surface charge transfer pathways. These results clearly demonstrate the importance of non-radical oxidation under alkaline conditions.

3.4. pH-dependent SED mechanism and environmental implications

Fig. 11 displays the pH-dependent decomplexation processes. At both acidic and alkaline pHs PDS activation by UV is the primary mechanism for the early decomplexation. As the reaction proceeds, the SED phenomenon occurs under both acidic and alkaline conditions. Nevertheless, in contrast to the conventional hypothesis, we demonstrate that the SED effect does not arise from the homogeneous Fenton-like catalysis of daughter Cu(II) species. Furthermore, the pH-dependent behavior in this study is not merely a difference in reaction rate, but reveals two distinct SED pathways governed by Cu speciation and catalytic form. Under acidic conditions (pH 3.0), SED effect mainly stems from the photochemical activity of daughter Cu(II) complexes and ligand-Cu(II)-PDS ternary complexes, which reduce Cu(II) to Cu(I). The produced Cu(I) complexes subsequently react with PDS to generate radicals. Meanwhile, the released ionic Cu^{2+} can jointly act as a catalyst to promote the decomplexation through $SO_4^{\bullet-}$ and Cu(III). In contrast, alkaline conditions exhibit no significant decomplexation enhancement by daughter Cu(II) complexes. Instead, the released labile Cu(II) undergoes spontaneous hydrolysis to form solid precipitates. Although the initially formed amorphous Cu(II) (hydr)oxides cannot effectively promote the decomplexation, they gradually transform into CuO nanosheets with considerable Fenton-like catalytic activity, enabling SED through PDS activation. Although decomplexation under alkaline conditions is slower than that under acidic conditions, the heterogeneous CuO precipitates can be reused for subsequent batches, retaining partial decomplexation activity. Conversely, such strategy is incompatible in acidic solution due to the acid-dissolution of the catalytically active precipitates below pH 5.5.

Further investigations of the decomplexation features of UV/PDS process were conducted by evaluating the decomplexation under different operational conditions. As shown in Fig. S19, increasing the initial Cu(II)-EDTA concentration prolonged both the induction stage and the time required for complete decomplexation under both acidic and alkaline conditions. When Cu(II)-EDTA concentration was below 0.1 mmol•L^{-1}, the induction stage was negligible. In contrast, increasing the PDS dosage enhanced the decomplexation rate (Fig. S20). A $[PDS]_0$:$[Cu(II)\text{-}EDTA]_0$ ratio of 50:1 was required to achieve nearly complete copper removal, a higher ratio than that for most pollutants. This is primarily due to the strong chelating ability of daughter ligands, which require multi-step degradation to release copper. Co-existing substance experiments revealed that sulfate and nitrate had minimal impact on the decomplexation under both acidic and alkaline conditions (Fig. 12). Chloride ions, however, slowed the process, with a more pronounced inhibitory effect under acidic conditions, likely due to the conversion of •OH into less reactive chlorine radicals. As discussed in the context, the importance of non-radical pathways is higher under alkaline conditions than under acidic conditions. The relatively weak oxidizing ability of the non-radical pathway enables it to resist the interference of chloride ions. The above results indicate that wastewater quality and treatment requirements are the key factors determining the decomplexation conditions.

4. Conclusions

In this study, we systematically revisited the decomplexation mechanism of Cu(II)-EDTA in the UV/PDS system, aiming to address the incompleteness and inconsistency of the conventional interpretation on the SED effect. The decomplexation behaviors and underlying mechanisms were investigated under both acidic and alkaline conditions to obtain a comprehensive understanding. Based on the results of light-dark cycling experiments and catalytic activity evaluation of various daughter Cu(II) species, we first verified that the conventional homogeneous autocatalysis hypothesis cannot explain the actual SED phenomenon. Instead, this work clearly demonstrates that the SED effect is directly governed by solution pH, leading to two fundamentally different decomplexation pathways. Under acidic conditions, the SED originates from UV-induced IET that generates Cu(I) species, which efficiently activate PDS to promote radical generation and Cu(II)/Cu(I) cycling. Under alkaline conditions, the SED is dominated by the in-situ hydrolysis, precipitation, and aging of labile Cu(II) species, forming CuO nanosheets with high heterogeneous Fenton-like activity toward PDS activation. These findings correct the misunderstanding of the SED mechanism and provide a more complete, pH-dependent mechanistic framework for Cu(II)-EDTA decomplexation in UV/PDS system. This study also offers a fundamental basis for the rational design and practical application of PDS-based advanced oxidation processes in treating copper-complex laden industrial wastewater.

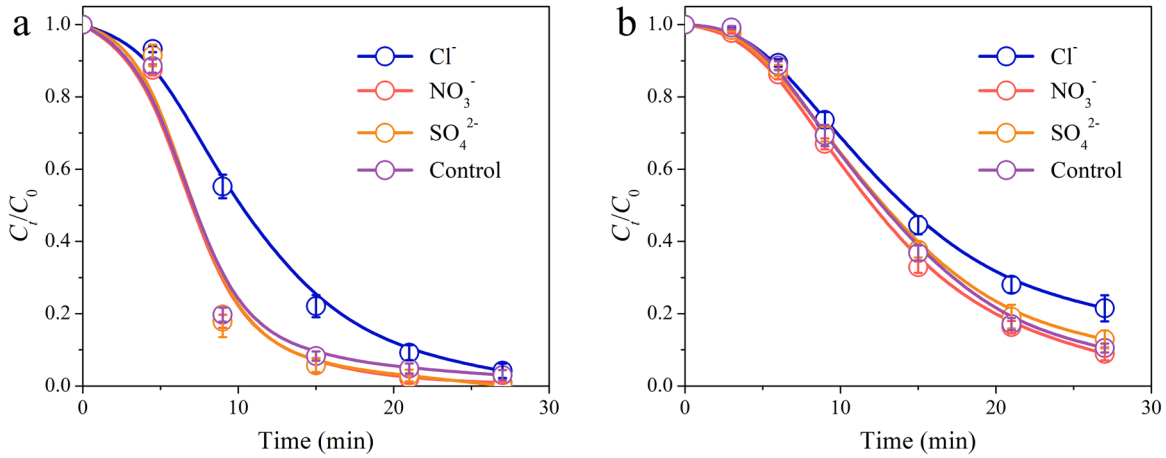

Fig. 12. Cu(II)-EDTA decomplexation in the presence of common co-existing anions ($[Cu(II)\text{-}EDTA]_0$ = 0.6 mmol•L^{-1}, $[PDS]_0$ = 50 mmol•L^{-1}, $[Cl^-]$ = $[NO_3^-]$ = $[SO_4^{2-}]$ = 3.0 mmol•L^{-1}).

CRediT authorship contribution statement

Zhe Xu: Writing – review & editing, Writing – original draft, Supervision, Investigation, Funding acquisition, Conceptualization. **Jiantong Zhou:** Writing – original draft, Investigation, Formal analysis, Data curation. **Chengfeng Liu:** Formal analysis, Data curation. **Weilan Zhen:** Data curation. **Taicheng An:** Supervision, Project administration.

Declaration of Competing Interest

The authors declare that they have no known competing financial interests or personal relationships that could have appeared to influence the work reported in this paper.

Acknowledgement

Financial support from the General Program of the National Natural Science Foundation of China (No. 22176130), the General Program of Guangdong Provincial Natural Science Foundation (No. 2023A1515010906), and the Qihang Program of Guangzhou Natural Science Foundation (No. 2025A04J3817) are gratefully acknowledged.

Appendix A. Supporting information

Supplementary data associated with this article can be found in the online version at doi:10.1016/j.jece.2026.123082.

Data availability

Data will be made available on request.

References

[1] F. Fu, Q. Wang, Removal of heavy metal ions from wastewaters: a review, J. Environ. Manag. 92 (2011) 407–418.
[2] Z. Xu, G. Gao, B. Pan, W. Zhang, L. Lv, A new combined process for efficient removal of Cu(II) organic complexes from wastewater: Fe(III) displacement/UV degradation/alkaline precipitation, Water Res. 87 (2015) 378–384.
[3] Z. Li, C. Du, Current status and research trends of electroplating wastewater treatment: systematic review and bibliometric analysis, Desalination 613 (2025) 119004.
[4] M. Li, N. Chen, H. Shang, C. Ling, K. Wei, S. Zhao, et al., An electrochemical strategy for simultaneous heavy metal complexes wastewater treatment and resource recovery, Environ. Sci. Technol. 56 (2022) 10945–10953.
[5] Q. Wang, Y. Li, Y. Liu, J. Ren, Y. Zhang, G. Qu, et al., Effective removal of the heavy metal-organic complex Cu-EDTA from water by catalytic persulfate oxidation: performance and mechanisms, J. Clean. Prod. 314 (2021) 128119.
[6] H. Zhang, L. Sun, S. Luo, R. Yuan, R. Hou, B. Zhou, et al., Electrode materials for copper removal from wastewater by bioelectrochemical systems: a review, J. Environ. Chem. Eng. 13 (2025) 116148.
[7] Z. Xu, Q. Zhang, X. Li, X. Huang, A critical review on chemical analysis of heavy metal complexes in water/wastewater and the mechanism of treatment methods, Chem. Eng. J. 429 (2022) 131688.
[8] Y. Zhu, W. Fan, T. Zhou, X. Li, Removal of chelated heavy metals from aqueous solution: a review of current methods and mechanisms, Sci. Total Environ. 678 (2019) 253–266.
[9] Y. Hong, Z. Luo, N. Zhang, L. Qu, M. Zheng, M.A. Suara, et al., Decomplexation of Cu(II)-EDTA by synergistic activation of persulfate with alkali and CuO: kinetics and activation mechanism, Sci. Total Environ. 817 (2022) 152793.
[10] Y. Wang, Y. Liu, B. Wu, M. Rui, J. Liu, G. Lu, Comparison of toxicity induced by EDTA-Cu after UV/H_2O_2 and UV/persulfate treatment: species-specific and technology-dependent toxicity, Chemosphere 240 (2020) 124942.
[11] W. Deng, X. Lv, Z. Xu, Q. Zhang, M. Zhao, X. Huang, Recovery of heavy metal complexes from wastewaters: a critical review of mechanisms and technologies, J. Environ. Manag. 382 (2025) 125339.
[12] M.J. Watts, K.G. Linden, Chlorine photolysis and subsequent OH radical production during UV treatment of chlorinated water, Water Res. 41 (2007) 2871–2878.
[13] X. Zhao, L. Guo, B. Zhang, H. Liu, J. Qu, Photoelectrocatalytic oxidation of Cu^{II}–EDTA at the TiO_2 electrode and simultaneous recovery of Cu^{II} by electrodeposition, Environ. Sci. Technol. 47 (2013) 4480–4488.
[14] S. Lan, Y. Xiong, S. Tian, J. Feng, T. Xie, Enhanced self-catalytic degradation of CuEDTA in the presence of H_2O_2/UV: evidence and importance of Cu-peroxide as a photo-active intermediate, Appl. Catal. B Environ. 183 (2016) 371–376.
[15] J. Li, J. Ma, R. Dai, X. Wang, M. Chen, T.D. Waite, et al., Self-enhanced decomplexation of Cu-organic complexes and Cu recovery from wastewaters using an electrochemical membrane filtration system, Environ. Sci. Technol. 55 (2021) 655–664.
[16] B. Shao, Y. Ren, H. Cai, J. Wang, Z. Zhou, J. Hu, et al., Autocatalytic decomplexation of Cu(II)-EDTA by unactivated peroxymonosulfate: the critical role of in situ complexes-assisted Cu(II) catalysis, J. Hazard. Mater. 498 (2025) 139978.
[17] J. Yu, W. Deng, X. Huang, M. Zhao, X. Li, T. Zhang, et al., Intramolecular generation of endogenous Cu(III) for selectively self-catalytic degradation of Cu (II)-EDTA from wastewater by UV/peroxymonosulfate, J. Hazard. Mater. 465 (2024) 133521.
[18] T. Zhao, J. Pan, C. Mao, L. Chen, J. Li, H. Shao, et al., Enhanced decomplexation of Cu-EDTA and simultaneous removal of Cu(II) by electron beam irradiation accompanied with autocatalytic fenton-like reaction: synergistic performance and mechanism, Chemosphere 313 (2023) 137445.
[19] Z. Xu, C. Shan, B. Xie, Y. Liu, B. Pan, Decomplexation of Cu(II)-EDTA by UV/persulfate and UV/H_2O_2: efficiency and mechanism, Appl. Catal. B Environ. 200 (2017) 439–447.
[20] Y. Liu, G. Qu, Q. Sun, H. Jia, T. Wang, L. Zhu, Endogenously activated persulfate by non-thermal plasma for Cu(II)-EDTA decomplexation: synergistic effect and mechanisms, Chem. Eng. J. 406 (2021) 126774.
[21] C. Wegeberg, O.S. Wenger, Luminescent first-row transition metal complexes, JACS Au 1 (2021) 1860–1876.
[22] H. Zhang, N. Li, Y. Wang, D. Zhao, J. He, H. You, et al., Real-time monitoring of the degradation of Cu(II)-EDTA in H_2O_2/UV using illumination-assisted droplet spray ionization mass spectrometry, Chemosphere 184 (2017) 932–938.
[23] C. Daniel, Electronic spectroscopy and photoreactivity in transition metal complexes, Coord. Chem. Rev. 238-239 (2003) 143–166.
[24] Y. Feng, R. Alonso-Mori, T. Barends, V. Blank, S. Botha, M. Chollet, et al., Demonstration of simultaneous experiments using thin crystal multiplexing at the Linac Coherent Light Source, J. Synchrotron Radiat. 22 (2015) 626–633.
[25] M.I. Franch, J.A. Ayllón, J. Peral, X. Domènech, Fe(III) photocatalyzed degradation of low chain carboxylic acids: implications of the iron salt, Appl. Catal. B Environ. 50 (2004) 89–99.
[26] D.A. Cagan, D. Bím, B. Silva, N.P. Kazmierczak, B.J. McNicholas, R.G. Hadt, Elucidating the mechanism of excited-state bond homolysis in nickel–bipyridine photoredox catalysts, J. Am. Chem. Soc. 144 (2022) 6516–6531.
[27] L. Chen, Z. Guo, X.-G. Wei, C. Gallenkamp, J. Bonin, E. Anxolabéhère-Mallart, Molecular catalysis of the electrochemical and photochemical reduction of CO_2 with earth-abundant metal complexes. Selective production of CO vs HCOOH by switching of the metal center, J. Am. Chem. Soc. 137 (2015) 10918–10921.
[28] X. Huang, Y. Wang, X. Li, D. Guan, Y. Li, X. Zheng, et al., Autocatalytic decomplexation of Cu(II)–EDTA and simultaneous removal of aqueous Cu(II) by UV/chlorine, Environ. Sci. Technol. 53 (2019) 2036–2044.
[29] D.A. Cagan, D. Bím, N.P. Kazmierczak, R.G. Hadt, Mechanisms of photoredox catalysis featuring nickel–bipyridine complexes, ACS Catal. 14 (2024) 9055–9076.
[30] Q. An, L. Chang, H. Pan, Z. Zuo, Ligand-to-metal charge transfer (LMCT) catalysis: harnessing simple cerium catalysts for selective functionalization of inert C–H and C–C bonds, Acc. Chem. Res. 57 (2024) 2915–2927.
[31] S. Wang, W. Zeng, Q. An, L. Duan, Z. Zuo, LMCT-driven electron relay unlocks alcohols as tunable reductants for nickel-catalyzed cross-electrophilic couplings, Nat. Commun. 16 (2025) 6162.
[32] J. Wellauer, M.L. Pattuwage, E.H. Doeven, T.U. Connell, O.S. Wenger, P.S. Francis, Rethinking the excited-state redox properties of iron (III) complexes for LMCT photoredox catalysis, J. Am. Chem. Soc. 147 (2025) 29304–29314.
[33] R. Chen, J. Wang, T. Huang, C. Zhang, X. Zhu, J. Li, F. Dong, Light-induced Fe-LMCT catalysis for redox-coupled conversion of NO_x and SO_2 mixture, Angew. Chem. 137 (2025) e202510456.
[34] Z. Xu, W. Zhen, C. Liu, J. Zhou, T. An, Robust decomplexation of Cu(II) complexes in excessive ligand environments by Mn(II)/PMS process: ligand concentration-dependent decomplexation mechanisms, J. Hazard. Mater. 507 (2026) 141833.
[35] X. Huang, Y. Xu, C. Shan, X. Li, W. Zhang, B. Pan, Coupled Cu(II)-EDTA degradation and Cu(II) removal from acidic wastewater by ozonation: performance, products and pathways, Chem. Eng. J. 299 (2016) 23–29.
[36] S. Sun, C. Shan, Z. Yang, S. Wang, B. Pan, Self-enhanced selective oxidation of phosphonate into phosphate by Cu(II)/H_2O_2: performance, mechanism, and validation, Environ. Sci. Technol. 56 (2022) 634–641.
[37] Z. Chu, Z. Han, H. Liu, T. Chen, X. Zou, H. Wang, et al., Autocatalytic degradation of Cu-EDTA in the Calcite/PMS system: singlet oxygen and Cu(III), J. Hazard. Mater. 477 (2024) 135286.
[38] Z. He, S. Yang, Y. Ju, C. Sun, Microwave photocatalytic degradation of Rhodamine B using TiO_2 supported on activated carbon: mechanism implication, J. Environ. Sci. 21 (2009) 268–272.
[39] Y. Ding, A. Sheng, J. Chen, Y. Deng, X. Cui, J. Liu, Regulatory mechanisms of carboxylic ligands with varying carboxyl group richness in Fe(II)-catalyzed ferrihydrite transformation, Geochim. Et. Cosmochim. Acta 409 (2025) 57–69.
[40] L. Wang, N. Jiang, H. Xu, Y. Luo, T. Zhang, Trace Cu(II)-mediated selective oxidation of benzothiazole: the predominance of sequential Cu(II)–Cu(I)–Cu(III) valence transition and dissolved oxygen, Environ. Sci. Technol. 57 (2023) 12523–12533.
[41] J.-R. Liu, G.-X. Xu, L.-G. Liu, S.-Q. Zhang, X. Hong, Recent advances in theoretical studies on Cu-mediated bond formation mechanisms involving radicals, ACS Catal. 14 (2024) 2429–2454.

[42] P.S. Rao, E. Hayon, Redox potentials of free radicals. I. Simple organic radicals, J. Am. Chem. Soc. 96 (1974) 1287–1294.
[43] C. Li, V. Goetz, S. Chiron, Peroxydisulfate activation process on copper oxide: Cu (III) as the predominant selective intermediate oxidant for phenol and waterborne antibiotics removal, J. Environ. Chem. Eng. 9 (2021) 105145.
[44] J. Liu, C. Ding, S. Gong, K. Fu, H. Deng, J. Shi, Enhanced Degradation of Antibiotic by Peroxydisulfate Catalysis with CuO@CNT: simultaneous $^1O_2$ Oxidation and Electron-Transfer Regime, Molecules 27 (2022) 7064.